Paper ID APEN-MIT-2020_198
Applied Energy Symposium: MIT A+B
May 17-19, 2020 • Cambridge, USA

Optimal Coordination of Distributed Energy Resources in Smart Grids Enabled by Distributed Optimization

Rabab Haider
Department of Mechanical Engineering
Massachussettes Institute of Technology
Cambridge, MA, USA
rhaider@mit.edu

Anuradha M. Annaswamy
Department of Mechanical Engineering
Massachussettes Institute of Technology
Cambridge, MA, USA
aanna@mit.edu

Abstract— **Modern active distribution grids are characterized by the increasing penetration of distributed energy resources (DERs). The proper coordination and scheduling of a large numbers of these small-scale and spatially distributed DERs can only be achieved at the nexus of new technological approaches and policies. As such, this paper presents a distributed optimal power flow formulation for the distribution grid, applied to the problem of Volt-VAR optimization (VVO). First, we propose a convex model to describe the power physics of distribution grids of meshed topology and unbalanced structure, based on current injection and McCormick Envelopes. Second, we employ the distributed proximal atomic coordination (PAC) algorithm, which has several advantages over other distributed algorithms, including reduced local computational effort and improved privacy. We implement VVO by optimally coordinating DERs including PV smart inverters and demand response. Results from the IEEE-34 bus network are presented, under different DER penetration scenarios and using different VVO objective functions. Our results show the need for DER coordination to achieve desired grid performance. Finally, we discuss the extension of such an optimal power flow formulation to the development of market derivatives to provide financial compensation to DERs providing grid services such as reactive power support and voltage support, within a local retail market framework.**

Keywords—smart grids, renewable energy integration, optimal power flow, distributed computation

I. Introduction

The modern distribution grid is characterized by the high penetration of distributed energy resources (DERs), which include distributed generation (DG), demand response (DR), and storage. These small-scale resources can provide various services to the grid, which include, but are not limited to, voltage support from clusters of DERs, reduced line congestion from better generation/load management, lower operating costs by using cheaper resources (ex. renewables), and demand flexibility by enabling DR throughout the distribution grid.

The large majority of these DERs are small-scale resources located behind-the-meter. In 2017, they contributed to 46.4GW of capacity on the US grid – almost 15% of peak summer load – and are expected to grow to over 100GW by 2023. The growth of these resources is led primarily by distributed solar (rooftop PV), DR from smart home appliances, and electric vehicles and home charging infrastructure. [1] Being positioned behind-the-meter, however, means they are not visible to utilities or control authorities. They are also largely owned by different third-party agents. These characteristics – the distributed nature, small scale, and third-party ownership – make the efficient integration of these resources into the grid a challenging and open research problem.

Resource coordination is typically done by solving the optimal power flow (OPF) problem, which determines the optimal power injections to minimize a cost metric subject to constraints which correspond to the power physics of the grid. The power physics equations are nonconvex, and typical convexification strategies assume radial topology and balanced structure of the grid [2]–[4]; the distribution grid however, is highly unbalanced due to the line characteristics and presence of unbalanced loads, and can have both radial and meshed topologies [5]. Further, the large number of these spatially distribution agents can render centralized approaches intractable, especially for online and real-time applications. Recent research efforts look towards decentralized and distributed approaches for optimization and decision making, enabled by the increased presence of grid-edge intelligence, computing resources, and peer-to-peer (P2P) communication networks (see [6]–[9] for reviews). Thus, there is a need for distributed algorithms built upon improved power systems models, which make decisions using local information without the aid of a central authority.

In this paper, we address these challenges by developing the necessary tools for distributed optimization in the distribution grid. The specific contributions are as follows:

- We propose a convex relaxation of the OPF problem based on current injection (CI) and McCormick Envelopes, which we leverage to model unbalanced distribution grids of general topologies. We extend this convex model to a distributed OPF algorithm based on the proximal atomic coordination (PAC) method.
- We implement distributed Volt-VAR optimization on the IEEE-34 node network, under different DER penetration. Results corroborate the need for distributed DER coordination to achieve desired grid performance, the need for DERs to provide reactive power support, and the need for financial compensation structures which price the locational and temporal variation of DER grid services.

This work was supported by the Department of Energy under Award Number DE-IA0000025 for UI-ASSIST Project.

The paper is organized as follows. Section II introduces notation, III describes the relaxed convex OPF problem, and IV introduces the PAC algorithm and properties of linear convergence. Section V describes the VVO problem setup for the IEEE-34 node network, for which results and discussion are presented in Section VI, and conclusions in Section VII.

II. Notation

We use x^R and x^I to denote the real and imaginary components of a complex number x; x^H is the Hermitian of vector x; overbar $\overline{x}$ and underbar $\underline{x}$ denote the upper and lower limits of a variable x; $\mathrm{Re}(\cdot)$ and $Im(\cdot)$ denote the real and imaginary components of a complex number. For a matrix $G \in \mathbb{R}^{n\times n}$, $[G]_{X_j}$ and $[G]^{X_j}$ denote the columns and rows of matrix G belonging to the jth partition of set X respectively, and G_{ij} to denote the entry at the ith row and j th column. We let $\lambda_{\min}(G)$, $\hat{\lambda}_{\min}(G)$, and $\lambda_{\max}(G)$ represent the smallest, smallest non-zero, and largest eigenvalue of G respectively.

We model the distribution network as an undirected graph of $\Gamma(N,\mathrm{E})$ with N nodes and M edges, where $N \coloneqq \{1,\dots,\mathrm{N}\}$ is the set of nodes of the grid, and $\mathrm{E} \coloneqq \{(m,n)\}$ is the set of edges. For a general 3-phase network, we denote each phase as $\phi \in \wp$ the set of phases. Each variable is thus a vector of 3 components, one for each phase $\phi \in \wp$. The 3-phase incidence matrix, $A \in \mathbb{R}^{3\mathrm{N}\times 3\mathrm{N}}$, describes the network topology, with positive outgoing edges and negative incoming edges. The nodal quantities are the real and reactive power injection (P_j, Q_j), voltage (V_j), and current injection (I_j). The current through the line is $I_{flow,ij} \forall (i,j) \in \mathrm{E}$. We use active sign convention, such that nodal injections are positive. Consider the nodal voltage, denoted as V_j^{ϕ} for node $j \in N$ and phase $\phi \in \wp$. We model the magnetic coupling between phases ϕ and ϕ' for a line between nodes i and j, using the 3-phase impedance matrix $Z_{ij} \in \mathbb{R}^{3\times 3}$. Each element $z_{\phi,\phi'}$ of Z_{ij} is $z_{\phi,\phi'} = R_{\phi,\phi'} + jX_{\phi,\phi'}, \forall \phi,\phi' \in \wp$. The system impedence matrix, Z, is the diagonal matrix composed of the line impedances.

III. Current Injection model

Denoting the column vector of line currents as I_{flow}, nodal voltages as V, and nodal current injections as I, the full current injection formulation (CI-OPF) is written as:

$$\min_x f(x) \tag{1a}$$
$$AV = ZI_{flow} \tag{1b}$$
$$I^R = \mathrm{Re}\left(A^T I_{flow}\right) \tag{1c}$$
$$I^I = \mathrm{Im}\left(A^T I_{flow}\right) \tag{1d}$$
$$\underline{V}_j^{\phi,R} \le V_j^{\phi,R} \le \overline{V}_j^{\phi,R} \quad \forall j \in N, \phi \in \wp \tag{1e}$$
$$\underline{V}_j^{\phi,I} \le V_j^{\phi,I} \le \overline{V}_j^{\phi,I} \quad \forall j \in N, \phi \in \wp \tag{1f}$$
$$\underline{P}_j^{\phi} \le P_j^{\phi} \le \overline{P}_j^{\phi} \quad \forall j \in N, \phi \in \wp \tag{1g}$$
$$\underline{Q}_j^{\phi} \le Q_j^{\phi} \le \overline{Q}_j^{\phi} \quad \forall j \in N, \phi \in \wp \tag{1h}$$
$$P_j^{\phi} = -V_j^{\phi,R} I_j^{\phi,R} + V_j^{\phi,I} I_j^{\phi,I} \quad \forall j \in N, \phi \in \wp \tag{1i}$$
$$Q_j^{\phi} = -V_j^{\phi,R} I_j^{\phi,I} + V_j^{\phi,I} I_j^{\phi,R} \quad \forall j \in N, \phi \in \wp \tag{1j}$$

where $x = [I^R \;\; I^I \;\; V^R \;\; V^I \;\; P \;\; Q]$ is the decision vector for the CI-OPF problem, (1b) describes Ohm's law, and (1c)-(1d) describe Kirchhoff's Current Law. The objective function (1a) is the performance index to be minimized, which can be, for example, to minimize cost for power production or line losses.

The OPF problem in (1) fully describes the power physics of an unbalanced network of either radial or meshed topology. However, constraints (1i)-(1j) render the problem nonconvex. We leverage convex relaxations, namely McCormick Envelopes (MCE) [10] to convert the bilinear terms to convex constraints. MCE denote a convex hull of a bilinear product $w = xy$ by utilizing the bounds on x and y. We denote this as:

$$\mathrm{MCE}\left(w, \underline{x}, \overline{x}, \underline{y}, \overline{y}\right) = \left\{w = xy : x \in \left[\underline{x}, \overline{x}\right], y \in \left[\underline{y}, \overline{y}\right]\right\},$$

and formally define it as:

$$M\left(w, \underline{x}, \overline{x}, \underline{y}, \overline{y}\right) = \begin{cases} w \ge \underline{x}y + x\underline{y} - \underline{x}\underline{y} \\ w \ge \overline{x}y + x\overline{y} - \overline{x}\overline{y} \\ w \le \underline{x}y + x\overline{y} - \underline{x}\overline{y} \\ w \le \overline{x}y + x\underline{y} - \overline{x}\underline{y} \end{cases} \tag{2}$$

We then introduce auxiliary variables $\{a,b,c,d\}$ to describe the bilinear terms in (1i)-(1j), and the corresponding linear constraints as described in (2). To do so, we must introduce current bounds, as defined in (3).

$$\underline{I}_j^{\phi,R} \le I_j^{\phi,R} \le \overline{I}_j^{\phi,R} \tag{3a}$$
$$\underline{I}_j^{\phi,I} \le I_j^{\phi,I} \le \overline{I}_j^{\phi,I} \tag{3b}$$

These are indirectly specified by (1e)-(1j), $\forall j \in N, \phi \in \wp$, and can be further calculated. The full relaxed CI model is then described by (1b)-(1h), (3a)-(3b), and the linear constraints for auxiliary variables as described in (2).

IV. Proximal Atomic Coordination Algorithm

In this section, we introduce the distributed algorithm of [11], [12], for the sake of completeness and comprehension. We first consider the following centralized optimization problem:

$$\min_y \sum_j f_j(y) \tag{4a}$$
$$\text{subj. to: } Gy = 0 \tag{4b}$$

where y is the decision vector, $f(y)$ is the objective function assumed to be a sum of separable functions, and matrix G represents the equality constraints, written in standard form.

We then decompose the central problem of (4) into J different coupled sub-optimization problems, which we call atomized problems, as in (5). The constraints and objective function are partitioned, with different decomposition profiles rendering different atomized formulations. Dependencies between each atom are treated by creating variable "copies": if atom A relies on a variable y_n owned by atom C, it creates a copy of the variable, denoted as y_n^A. Coordination constraints of the form $y_n^A - y_n = 0$ are introduced in atom A, which drive the variable copy to the true value, through communication with atom C. These can be compactly represented by constraint $[B]^j a = 0$ for an atom $j \in J$.

$$\min_{a_j} \sum_j f_j(a_j) \tag{5a}$$

$$\text{subj. to: } G_j a_j = 0 \quad \forall j \in J \tag{5b}$$

$$[B]^j a = 0 \quad \forall j \in J \tag{5c}$$

A. Algorithm Specifications

We first form the atomic Lagrangian function for (5):

$$\begin{aligned}\mathcal{L}(a,\mu,\nu) &= \sum_{j\in J}\left[f_j(a_j) + \mu_j^T G_j a_j + \nu_j^T [B]^j a\right] \\ &= \sum_{j\in J}\left[f_j(a_j) + \mu_j^T G_j a_j + \nu^T [B]_j a_j\right] \\ &= \sum_{j\in J} \mathcal{L}_j(a_j,\mu_j,\nu)\end{aligned} \tag{6}$$

We can then apply the prox-linear approach of [13] to (6), to ensure parallel computation of each primal step, and obtain the PAC algorithm:

$$a_j[\tau+1] = \operatorname{argmin}\left\{\mathcal{L}_j(a_j,\hat{\mu}_j[\tau],\hat{\nu}[\tau]) + \frac{1}{2\rho}\|a_j - a_j[\tau]\|_2^2\right\} \tag{7}$$

$$\mu_j[\tau+1] = \mu_j[\tau] + \rho\gamma_j G_j a_j[\tau+1] \tag{8}$$

$$\hat{\mu}_j[\tau+1] = \mu_j[\tau+1] + \rho\,\hat{\gamma}_j[\tau+1] G_j a_j[\tau+1] \tag{9}$$

$$\text{Communicate } a_j \forall j \in J \text{ with neighbours} \tag{10}$$

$$\nu_j[\tau+1] = \nu_j[\tau] + \rho\gamma_j [B]^j a[\tau+1] \tag{11}$$

$$\hat{\nu}_j[\tau+1] = \nu_j[\tau+1] + \rho\hat{\gamma}_j[\tau+1][B]^j a[\tau+1] \tag{12}$$

$$\text{Communicate } \hat{\nu}_j \forall j \in J \text{ with neighbours} \tag{13}$$

B. Convergence Results

We make the following assumptions on the structure of the central and atomized formulations, where $\gamma_{\min} \triangleq \min_{j\in K}\{\gamma_j\}$, $\tilde{G} = \operatorname{diag}(G_j)_{\forall j \in J}$, and $R^\Gamma R^\Gamma = \tilde{G}^T \Gamma^{\tilde{G}} \tilde{G} + B^T \Gamma^B B$:

- Each $f_j \; \forall j \in J$ is a closed, convex and proper (CCP) function with $\operatorname{dom}(f_j) = \mathbb{R}^Y$, and is differentiable, α-strongly convex and L-strongly smooth.
- There exists a non-trivial optimal solution to the central problem (4), y^*. The optimal atomized solution a^* is related to y^* via a projection $y^* = \Pi^L a^*$.
- Let the PAC parameters satisfy:

  $1 \geq \rho^2 \gamma_{\min} \lambda_{\max}(\tilde{G}^T \tilde{G} + B^T B)$

If these assumptions hold, and the PAC parameters satisfy $\rho > 0$ and $\gamma_j > 0$ for $1 \leq j \leq K$, and let:

$$a[\tau] = [a_1[\tau]; \cdots; a_K[\tau]],$$

represent the PAC trajectory of (7)-(13) under zero initialization. Then there exists a unique optimal atomized solution such that, for all τ:

$$\lim_{t\to\infty}\{a[\tau]\} = a^*$$

and linear convergence with:

$$\|a[\tau] - a^*\| \leq [1 + \zeta_P(\rho,\gamma_{\min})]^{-\tau}\left(\|a^*\|^2_{\tilde{V}_2(\rho,\Gamma)} + \|r^*\|_2^2\right)$$

where:

$$\zeta_P(\rho,\gamma_{\min}) = \frac{2\alpha\rho\gamma_{\min}\tilde{\lambda}_{\min}(V_1)}{2\alpha L + 2\rho^{-2} + \gamma_{\min}\tilde{\lambda}_{\min}(V_1)} \tag{14}$$

with $r^* \in \mathbb{R}^{|T|}$ satisfying:

$$R^{\Gamma r^*} + \frac{1}{\rho}\nabla_a \hat{f}(a) = 0.$$

The proof and additional details are in [11], [12].

V. Application to Volt-VAR Optimization

We apply the distributed OPF developed using CI and PAC to the problem of VVO in distribution girds with high penetration of DERs. The highly temporal and spatial nature of DERs suggests a need for finer grain control of the voltage profile, which cannot be met through the use of traditional voltage regulators and capacitor banks. We assume protection schemes are well designed and will correct the system if a fault event occurs. We model the IEEE-34 bus network (see Figure 1), a 3-phase unbalanced distribution feeder. Switches are assumed in their normal positions, and line loads are converted to spot loads by equally distributing them between the connecting nodes. The capacitor banks are modelled as negative reactive power generators, with continuous operating range between 0 and full capacity. We modify the network by adding DERs at different nodes.

A. Modeling DERs

We perform VVO at the secondary feeder, where each node is a single residential unit. We model three types of DERs: DR units, DGs, and prosumers, each detailed below.

1) Demand Response: Flexible loads are modelled with different demand response percentages, denoted as $DR_i\%$, where $0 \leq DR_i\% \leq 1$ and $\overline{P_i} = \underline{P_i} \times (1 - DR_i\%)$, by active sign convention. For inflexible loads, $\underline{P_i} = \overline{P_i}, \overline{P_i} \leq 0$. We assume the reactive power of all consumers are fixed, $\underline{Q}_i = \overline{Q}_i, \overline{Q}_i \leq 0$.

2) Distributed Generation: Distributed generators are rooftop PV units rated at 4-10kW capacity, denoted by P_i^{Cap}, which is the typical range for residential PV in the US. Hourly generation forecasts were obtained from the NREL System Advisory Model (SAM) tool, using the small scale distributed residential PV model, queried for May 14 [14]. The generation data[2] is normalized to render generation profile $\alpha_{PV}(t)$ to be used for all PV units throughout the network; we assume the solar irradiance over the entire network is equal. We assume all renewable generation can be curtailed, and that all units are equipped with smart inverters capable of adjusting power factor[3]. We do not consider storage in this work. The full model for a PV unit at node j is:

$$\underline{P_j} = 0, \overline{P_j}(t) = \alpha_{PV}(t) \mathrm{P_j^{Cap}}, \underline{Q_j} = -\overline{Q}_j \tag{15a}$$

$$P_j \tan(\cos^{-1}(-\mathrm{pf})) \leq Q_j \leq P_j \tan(\cos^{-1}(\mathrm{pf})) \leq Q_j \tag{15b}$$

[2] We use data from Phoenix, AZ, using the SunPower SPR-X21-335 module, and a single inverter (SMA America, SB3800TL-US-22, 240V). The DC to AC ratio is set to the default of 1.2.

[3] Rule 21 in CAISO requires that all distributed generators be equipped with smart inverters, as of 2014.

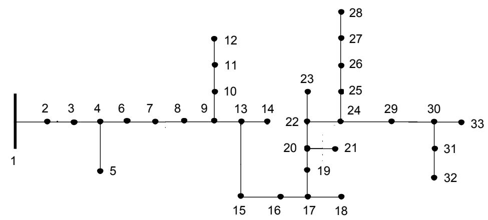

Fig. 1: IEEE-34 node network topology, with node 1 the PCC

3) Prosumers: Prosumers are nodes where both load and generation are present. To model each device properly, we must introduce additional variables representing the load and generation powers[4]:

$$P_j = P_j^G - P_j^L, \qquad P_j^G \geq 0, P_j^L \geq 0 \tag{16a}$$

$$Q_j = Q_j^G - Q_j^L, \qquad Q_j^L \geq 0 \tag{16b}$$

$$\overline{P}_j = \overline{P}_j^G - \underline{P}_j^L, \qquad \underline{P}_j = \underline{P}_j^G - \overline{P}_j^L \tag{16c}$$

$$\overline{Q}_j = \overline{Q}_j^G - \underline{Q}_j^L, \qquad \underline{Q}_j = \underline{Q}_j^G - \overline{Q}_j^L \tag{16d}$$

The PV generator located at a prosumer node j will be represented by the equations in (15), with all P_i and Q_i variables replaced by the P_i^G and Q_i^G. Similarly, loads located at prosumer node j (including demand response) will replace $\underline{P}_i$ and $\underline{Q}_i$ variables with P_i^L and Q_i^L but with $\underline{P}_i^L = -\overline{P}_i$ and $\overline{P}_i^L = -\underline{P}_i$.

B. Simulation Setup

We run simulations for 24 hours with nodal loads varying as per profiles $\alpha_j^{\mathrm{P}}(t)$ and $\alpha_j^{\mathrm{Q}}(t)$ for real and reactive power respectively. The baseline time-dependent load ratio $\alpha_D(t)$ varies according to the ISO-NE report of total recorded electricity demand for each five-minute interval of May 14, 2019 [15]. This ratio is perturbed to obtain the ratio per node $j, \alpha_j(t)$, where $\alpha_j(t) = \alpha_D(t)\delta_j^P$ with $\delta_j^P \sim \mathrm{N}(0, \sigma_P)$, and the resulting profile is smoothed. The same is done for reactive power Q. We select $\sigma_P = 0.1$ and $\sigma_Q = 0.01$ to ensure P and Q load profiles are not identical.

1) Test Cases: To test the performance of the CI model and PAC algorithm, we consider varying penetration of DERs through the four cases below:

- Case A: [Baseline] time-varying loads and shunt capacitors with IEEE-34 configuration
- Case B: [DR] Baseline case with DR present in the grid
- Case C: [PV] Baseline case with PV units with smart inverters and adjustable power factor
- Case D: [Combination] Baseline case with DR and PV

To compactly represent the different DER scenarios, we make use of a case notation. For cases A, B, and C, the scenarios follow the notation *X_XX_XX* as below. For case B, the low DR case (20% penetration) takes all units with $10\% - 30\%$ curtailable load at all hours of the day. In the high DR case (50% penetration), all units have $50\% - 80\%$ curtailable load at all hours of the day.

- X: {A,B,C} Case code
- XX: {20,40,50,60} penetration of the resource through network as % of nodes with specific DER capabilities
- XX: {1,95,90,80} For case C: minimum pf setting of all PV units (with 1 for fixed unity pf)

The scenarios for case D follow the notation *D_XX_XX* as below, with all PV units having minimum pf of 0.9. All DR units have 10%–30% curtailable load at all hours of the day[5].

- XX: {40,60} penetration of PV units through network as % of nodes with PV
- XX: {20,50} penetration of DR through network as % of nodes with DR capabilities

2) Objective Function: We consider three different objective functions to achieve VVO in the distribution grid:

- I. Regulate voltage about a prior set-point:

$$f(a) = \sum_{j\in J}\sum_{\phi\in\mathcal{P}}\left[(V_j^{\phi,R} - \tilde{V}_j^{\phi,R})^2 + (V_j^{\phi,I} - \tilde{V}_j^{\phi,I})^2\right]$$

- II. Minimize line losses:

$$f(a) = \sum\nolimits_{j\in J}\sum\nolimits_{\wp} R_{j,k}\left[{I_{flow,ij}^R}^2 + {I_{flow,ij}^I}^2\right]$$

- III. Minimize feeder power import:

$$f(a) = P_{j^\#}$$

For function I, $\tilde{V}_j^{\phi,R}$ and $\tilde{V}_j^{\phi,I}$ are the desired setpoints, which for our case study we take $\tilde{V}_j^{\phi,R} = 1$, and $\tilde{V}_j^{\phi,I} = 0, \forall j \in J \setminus j^\#, \phi \in \wp$. We note that node $j^\#$ which is the point of common coupling (PCC) to the transmission grid is treated as a slack node, with $V_{j^\#}^{\phi,R} = 1$ and $V_{j^\#}^{\phi,I} = 0, \forall\, \phi \in \wp$. For function II, the resistance $R_{j,k} \in \mathbb{R}^{3\times3}$, and branch currents $I_{flow,ij} \in \mathbb{R}^{3\times1}$ for both real and imaginary components, to account for the magnetic interaction between phase ϕ and ϕ'. The squared operator acts element-wise, and the inner summation acts as a mapping to sum the elements together.

VI. Results and Discussion

In this section we present the simulation results of VVO on the different test cases. All simulations were performed on a 2.3 GHz Intel Core i5 machine using MATLAB, with optimization problems being setup using the YALMIP interface [17], and solved directly with Gurobi Optimizer.

The parameters $\rho, \gamma, \hat{\gamma}_j$ of the PAC algorithm were tuned to guarantee algorithm convergence (see [11], [12] for details).

A. Voltage Results

The resulting voltage bounds are presented in Fig. 2 for each of the test cases. The voltage bounds are calculated by finding the minimum and maximum voltage across all nodes and all time (24 hour simulation), and the average voltage (denoted by the dot on the range) is similarly calculated across all nodes and time. The simulations specify very loose

[4] For these variables, we do not use active sign convention

[5] A demand response potential survey for Bonneville Power Administration [16] indicated achievable DR levels of 15% in winter and 64% in summer, with 10% DR easily achievable among public utilities in RTOs. The report also suggests small utilities can achieve up to DR potentials of 50% peak load. We simulate 10%-30% capabilities to test future extreme DER penetration scenarios.

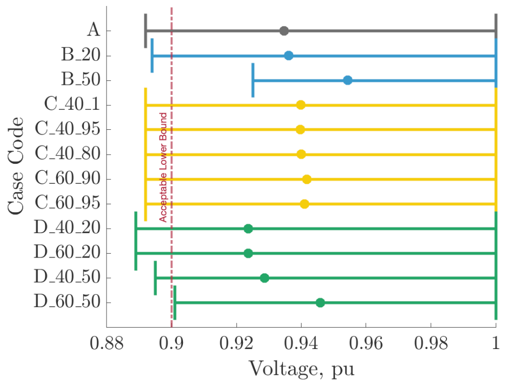

Fig. 2: Results for the IEEE-34 node network with Objective I and varying test cases. The bars indicate the range of voltage, and the dot indicates the average voltage in the network over space and time.

voltage bounds of $V_j \in [0.85, 1.15]$ pu, to ensure the optimization problem is always feasible. Through the coordination of DERs, the lower voltage bound should be pushed into the acceptable operating range of ±10%, which corresponds to $V_j \in [0.9, 1.1]$pu, as denoted in the figure, with narrower operating bounds and averages closer to 1pu being preferred[6].

The baseline case (Case A, in grey) clearly shows that the network exhibits low voltage problems despite having shunt capacitors, with the minimum voltage below 0.9pu, and an average below 0.94pu. The results for Case B (in blue) show that the use of DR can boost grid voltages by reducing the total network load. However, a substantial voltage increase is only achieved in Case B 50, where DR has very high penetrations and upwards of 50%-80% of the load can be curtailed. This is an unrealistic level of curtailable load and suggests the need for other resources. The results for Case C (in yellow) show minimal improvement from the baseline case, with the average only marginally improved but still below the acceptable limits in North America. This can be explained by the variable nature of solar generation, where solar power is not available at all hours of the day. The simulation data has nonzero generation between hours 7 and 20, while the average load profile shows the maximum load occurring between hours 18 and 22. Thus, the low voltage issues in the network caused by the high evening demand cannot be addressed through the use of PV inverters. Finally, the results for Case D show how both DR and PV with smart inverters can be leveraged to improve grid voltages, with reasonable DER levels. The DR units increase the minimum voltage and can be used during all hours of the day; while the PV units boost the average voltage, primarily through reactive power support.

B. Resource Utilization

To better understand the spatial-temporal use of the different DERs, we consider resource utilization factors. These are calculated as below, with the variables for prosumers being changed for DR and PV utilization to P_j^L and P_j^G respectively.

[6] Voltage standards detailing the allowable deviation from nominal voltage under normal grid conditions vary globally. North America follows ANSI C84.1 which allows ±5% deviation, while Europe follows IEC and European EN 50160 which allows ±10% deviation. We consider the European voltage bounds as they provide more flexibility in operations.

- DR Utilization: $\frac{\text{curtailed load}}{\text{curtailable load}} = \frac{\Sigma_{\phi\in\wp}(|\underline{P}_j^{\phi}| - |P_j^{\phi*}|)}{\Sigma_{\phi\in\wp}\left(|\underline{P}_j^{\phi}| - |\overline{P}_j^{\phi}|\right)}$
- PV Utilization: $\frac{\text{generation setpoint}}{\text{variable generation capacity}} = \frac{\Sigma_{\phi\in\wp} P_j^{\phi*}}{\Sigma_{\phi\in\wp}\left(\overline{P}_j^{\phi} - \underline{P}_j^{\phi}\right)}$
- Power Factor: $\cos\left(\arctan\frac{\Sigma_{\phi\in\wp} Q_j^{\phi*}}{\Sigma_{\phi\in\wp} P_j^{\phi*}}\right)$

The results are shown as heat maps in Fig. 3 for Cases B and C, and Fig. 4 for Case D. The x-axis denotes the hour of the day (1 thru 24). The y-axis identifies the location of the resource by node number. For prosumers, the node number is annotated with 'G' and 'L' in subscripts, to indicate generation and load at the node respectively. DR utilization is shown from white to red (-1 to 0) and PV utilization is shown from white to blue (0 to 1), with darker colours corresponding to higher resource utilization. Power factor is measured from the minimum allowable to unity. The 'NaN' value indicates the resource was not available at the time.

For Case B (Fig. 3a), the striking red across the entire map shows that DR units are used at full capacity at all hours of the day, to boost the grid voltage by reducing network load, as can be expected from the voltage results in Fig. 2. For Case C, results are shown for low penetration of PV

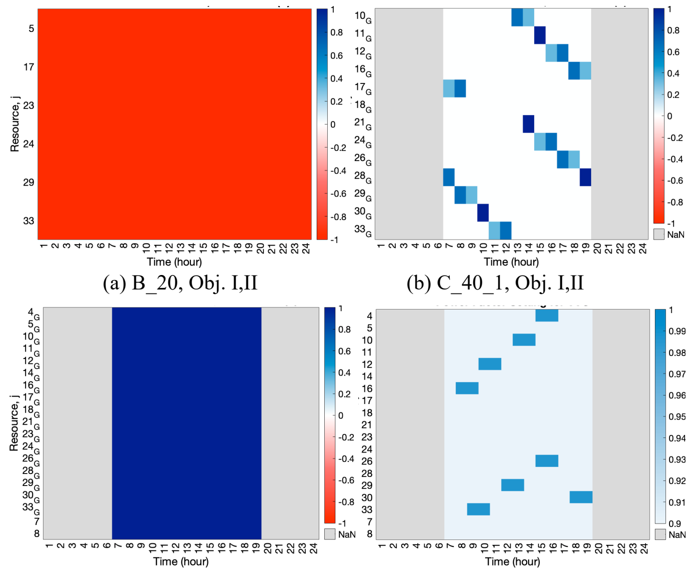
(a) B_20, Obj. I,II (b) C_40_1, Obj. I,II

(c) C_60_90, Obj. I,II (d) C_60_90, Obj. I,III

Fig. 3: Resource utilization (a-c) and power factor (d) heat maps, Cases B and C

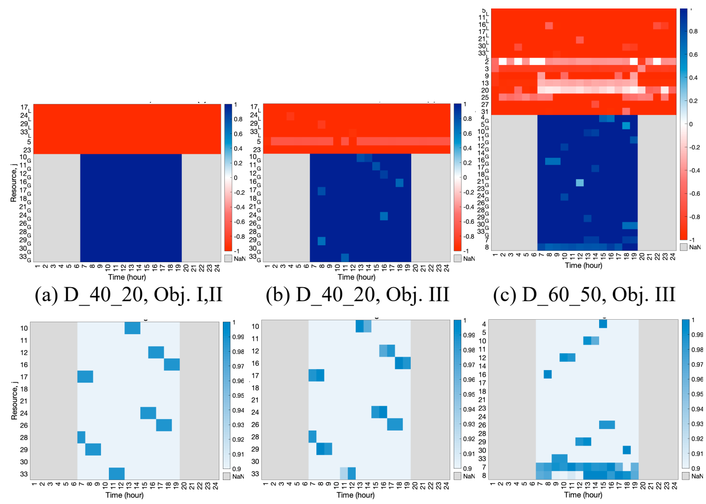
(a) D_40_20, Obj. I,II (b) D_40_20, Obj. III (c) D_60_50, Obj. III

(d) D_40_20, Obj. I,II (e) D_40_20, Obj. III (f) D_60_50, Obj. III

Fig. 4: Resource utilization (top) and power factor (bottom) heat maps for Case D

(40%) with fixed unity power factor (Fig. 3b), and a high penetration of PV (60%) with a minimum power factor of 0.9 (Fig. 3c and 3d). For fixed unity power factor case, the PV generation is mostly curtailed, while for variable power factor case the PV generation is never curtailed, and is used most frequently to supply reactive power. This is indicated by the lighter blue squares in the pf map (Fig. 3d). This shows the need for DERs capable of reactive power support, even in networks with traditional resources like capacitor banks and on-load tap changers (OLTC) transformers. The maps for Case D compare the use of different objective functions in Fig. 4a,4d and Fig. 4b,4e – all resources are being utilized at near full capacity, but the different objective functions render different resource utilization. This shows the need for assessing the requirements of each network and selecting tailored objectives to conduct VVO. A comparison of Fig. 4b,4e and Fig. 4c,4f, which use the same objective function, shows how resource utilization changes with DER penetration – in the second case, some PV generation is curtailed and some DR units are not leveraged; further, generators at nodes 7 and 8 provide mostly real power while other units provide mostly reactive power.

C. *Future Work: Extensions to Distribution-Level Markets*

The results presented here clearly show that appropriate coordination of DERs can achieve VVO in the distribution grid. These resources are providing grid services in the form of load curtailment, energy exports, and power factor modulation. For providing these services, DERs must be financially compensated. Existing policies for DER compensation (including retail DR programs and net energy metering) fall short of yielding efficient investment and operations of distribution systems as they do not typically price the locational and temporal variation in the services DERs provide - these variations are clearly shown in the resource utilization maps and power factor maps of (Fig. 3, 4). Further, programs which compensate DERs for voltage support or reactive power support do not exist. This suggests the need for new market derivatives.

Despite increased DER participation at the wholesale level (such as through FERC Order 841 for storage, Orders 719 and 745 for DR, and interconnection procedures such as WDAT in California), as the number of small-scale DERs in the distribution grid grows, the WEM alone may not suffice in realizing efficient and reliable power delivery. Rather, a retail market which oversees the scheduling and compensation of DERs is highly necessary. In [18], transactive energy schemes are at the core of a retail market coordinated by a Distribution System Operator. The proposed retail market leverages the PAC algorithm to solve the optimal power flow, with its solution serving as the schedule and retail prices for DERs in an energy market.

We propose the use of the distributed CI model based on the PAC algorithm to extend the retail market in [18]. By fully describing the power physics for unbalanced networks, appropriate market derivates to achieve VVO through the coordination of DERs can be developed. This will be analyzed in future work. Further, there is a need for a cyber framework upon which these DERs can be coordinated – we propose a service-oriented broker architecture (SOBA) that conceptualizes such a framework in [19]. By treating the grid as a multiagent system, the DERs can be coordinated by system operators through service requests, using such structures as the retail market. Additional future work includes the deployment of the extended retail market on a cyber-physical testbed, comprised of the SOBA platform.

VII. Concluding Remarks

In this work, we achieve distributed VVO in unbalanced distribution grids, through the optimal coordination of DERs, namely DR and rooftop PV with smart inverters. We leverage the recently proposed PAC algorithm to solve the convex CI power flow model, and present simulation results for the IEEE-34 node network. The results clearly show that DERs can be used to achieve VVO, through the provision of spatial and temporally varying grid services.

References

[1] J. S. John, "Distributed energy poised for 'explosive growth' on the us grid," June 2018.

[2] M. Farivar and S. Low, "Branch flow model: Relaxations and convexification," *2014 IEEE PES TD Conference and Exposition*, 2014.

[3] L. Gan, N. Li, U. Topcu, and S. H. Low, "Exact convex relaxation of optimal power flow in radial networks," *IEEE Transactions on Automatic Control*, vol. 60, pp. 72–87, Jan 2015.

[4] J. Lavaei and S. H. Low, "Zero duality gap in optimal power flow problem," *IEEE Transactions on Power Systems*, vol. 27, no. 1, p. 92–107, 2012.

[5] W. H. Kersting, Distribution system modeling and analysis. CRC press, 2006.

[6] D. K. Molzahn, F. Dorfler, H. Sandberg, S. H. Low, S. Chakrabarti,¨ R. Baldick, and J. Lavaei, "A survey of distributed optimization and control algorithms for electric power systems," *IEEE Transactions on Smart Grid*, vol. 8, no. 6, pp. 2941–2962, 2017.

[7] J. M. Guerrero, M. Chandorkar, T. Lee, and P. C. Loh, "Advanced control architectures for intelligent microgrids—part i: Decentralized and hierarchical control," *IEEE Transactions on Industrial Electronics*, vol. 60, no. 4, pp. 1254–1262, 2013.

[8] F. F. Wu, K. Moslehi, and A. Bose, "Power system control centers: Past, present, and future," *Proceedings of the IEEE*, vol. 93, no. 11, pp. 1890–1908, 2005.

[9] M. Yazdanian and A. Mehrizi-Sani, "Distributed control techniques in microgrids," *IEEE Transactions on Smart Grid*, vol. 5, no. 6, pp. 2901– 2909, 2014.

[10] G. P. Mccormick, "Computability of global solutions to factorable nonconvex programs: Part i — convex underestimating problems," *Mathematical Programming*, vol. 10, no. 1, p. 147–175, 1976.

[11] J. Romvary, G. Ferro, R. Haider, and A. Annaswamy, "A distributed proximal atomic coordination algorithm," *IEEE Transactions on Automatic Control*, 2020 (provisionally accepted).

[12] J. Romvary, A proximal atomic coordination algorithm for distributed optimization in distribution grids. PhD thesis, Massachusetts Institute of Technology, 2018.

[13] G. Chen and M. Teboulle, "A proximal-based decomposition method for convex minimization problems," *Mathematical Programming*, vol. 64, pp. 81–101, Mar 1994.

[14] National Renewable Energy Laboratory, "System advisory model." https://sam.nrel.gov/, 2020.

[15] ISO-NE, "Energy, load, and demand reports." https://www.iso-ne.com/ isoexpress/web/reports/load-and-demand/-/tree/dmnd-five-minute-sys, 2019.

[16] H. Haeri, L. Garth, J. Wang, J. Stewart, M. Osborn, S. Shaw, M. Knipe, J. Kennedy, J. Abromowitz, H. Javanbakht, T. Bettine, H. Ratcliffe, D. Vaughn, and S. Spencer, "Demand response potential in bonneville power administration's public utility service area," Sept 2019.

[17] J. Lofberg, "Yalmip : A toolbox for modeling and optimization in¨ matlab," in *In Proceedings of the CACSD Conference*, (Taipei, Taiwan), 2004.

[18] R. Haider, S. Baros, Y. Wasa, J. Romvary, K. Uchida, and A. Anaswamy, "Towards a retail market for distribution grids," *IEEE Transactions on Smart Grids*, 2020. doi: 10.1109/TSG.2020.2996565.

[19] M. B. Bah, R. Haider, V. Venkataramanan, and A. M. Annaswamy, "Toward a service-oriented broker architecture for the distribution grid," *Smart Grids Comm 2020*, 2020 (to be published).